SAND2018-13567C

Ultra-high-speed Pulse-burst Phase Conjugate Digital In-line Holography for Imaging Through Shock-wave Distortions

Yi Chen*, Jeffery D. Heyborne†, and Daniel R. Guildenbecher‡
Sandia National Laboratories, Albuquerque, NM 87185, USA.

Michael E. Smyser§ and Mikhail N. Slipchenko¶
Purdue University, West Lafayette, IN, 47907, USA.

Digital in-line holography techniques for coherent imaging are important for object sizing and tracking applications in multiphase flows and combustion systems. In explosive, supersonic, or hypersonic environments, however, gas-phase shocks impart phase distortions that obscure objects. In this work, we implement phase-conjugate digital in-line holography (PCDIH) with both a picosecond laser and a nanosecond pulse-burst laser for reducing the phase distortions caused by shock-waves. The technique operates by first passing a forward beam of coherent light through the shock-wave phase-distortion. The light then enters a phase-conjugate mirror, created via a degenerate four-wave-mixing process, to produce a return beam with the opposite phase-delay as the forward beam. By passing the return beam back through the phase-distortion, phase delays are canceled producing phase-distortion-free images. This technique enables the measurement of the three-dimensional position and velocity of objects through shock-wave distortions at rates up to 500 kHz. This method is demonstrated in a variety of experiments including imaging supersonic shock-waves, sizing objects through laser-spark plasma-generated shock-waves, and tracking explosively-generated hypersonic fragments.

I. Introduction

Digital in-line holography (DIH) is a coherent imaging method that can be used for three-dimensional (3D) object tracking along a single line-of-sight with a single laser-pulse [1, 2]. It has various practical applications from studying high speed objects in flow [3–8] and combustion [9–13] environments. However, because DIH records the interference pattern of laser light, it is susceptible to phase disturbances generated by shock-waves in supersonic, hypersonic, and explosive environments. This makes implementation of traditional DIH impractical for these applications.

One method for eliminating phase distortions is to use a phase-conjugate mirror as illustrated in Fig. 1. A phase disturbance picked up by the imaging beam can be reversed in a phase-conjugate mirror to produce a backward propagating beam with the opposite phase. This beam then passes back through the phase object, which cancels the phase distortion. Phase conjugate techniques have been applied to remove imaging distortions [14–17] as well as minimize amplified spontaneous emission and modal dispersion [18, 19]. Similar techniques for holography have also been applied using film [20] and spatial light modulators [21–23]. However, these techniques for generating phase-conjugate mirrors are slow and cannot be applied in ultra-high-speed environments. Techniques which implement phase conjugate digital in-line holography (PCDIH) with degenerate four-wave-mixing [24, 25], however, are compatible with ultra-high-speed applications. Previous work, however, has been limited to 10 to 20 Hz repetition rates [24, 25]. For extreme environments, such as explosive tests, this would only enable one frame to be captured per test.

With recent developments in pulse-burst lasers for operation at hundreds of kilohertz (kHz) to megahertz (MHz), however, more than a single frame can be captured per test. Pulse-burst lasers have been recently applied to transonic wind tunnels for particle image velocimetry [26], turbulent flame environments for laser induced incandescence [27, 28], and time-resolved temperature measurements using coherent anti-Stokes Raman scattering spectroscopy [29]. High power [30] and megahertz rate [31] pulse-burst laser systems have also been constructed. New ultra-high-speed camera technologies have also demonstrated frame rates of 5 MHz or more [32].

*Post-Doctoral Appointee, Engineering Sciences Center, yichen@sandia.gov, Member AIAA.
†Electromechanical Technologist, Explosive Technologies Group, jdheybo@sandia.gov.
‡Principal Member of the Technical Staff, Engineering Sciences Center, drguild@sandia.gov, Member AIAA.
§Ph.D. Student, School of Mechanical Engineering, msmyser@purdue.edu, Member AIAA.
¶Research Associate Professor, School of Mechanical Engineering, mslipche@purdue.edu, Member AIAA.

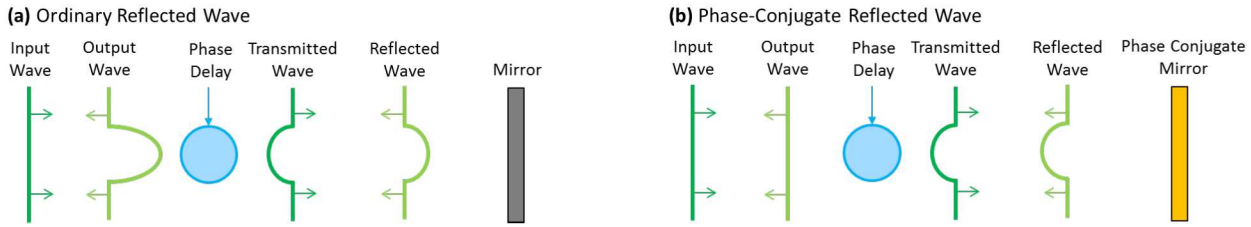

Fig. 1 Distortions produced by phase objects, such as a shock-wave, are illustrated for configurations with (a) an ordinary mirror and (b) a phase-conjugate mirror.

By combining PCDIH with pulse-burst lasers and ultra-high-speed cameras, it is now possible to capture time-resolved data from extreme environments. In this work, we describe a new ultra-high-speed PCDIH imaging technique that operates at up to 500 kHz for recording holograms in explosive, supersonic, and hypersonic environments. We describe the theoretical foundations and experimental setup required to achieve the measurement. Results illustrating the ability to cancel distortions from stationary supersonic shock-waves, laser-spark plasma-generated shock-waves, and explosively-generated hypersonic fragments are then discussed.

II. PCDIH with Degenerate Four-wave Mixing

A. Phase-Conjugate Mirror

The operating principle of a phase-conjugate mirror can be compared with a normal mirror in Fig. 1 by starting with an input wave of the form, $E(x,y,z) = A_0(x,y,z)e^{ikz-i\omega t}$. When this input wave passes through the phase disturbance the transmitted wave picks up a phase delay ϕ such that, $E'(x,y,z) = A_0(x,y,z)e^{ikz+i\phi(x,y,z)-i\omega t}$. With the conventional mirror with reflectivity R_m, the reflected wave and output wave after passing through the phase delay a second time are,

$$E''(x,y,z) = R_m A_0(x,y,z)e^{-ikz+i\phi(x,y,z)-i\omega t}, \tag{1}$$

$$E'''(x,y,z) = R_m A_0(x,y,z)e^{-ikz+2i\phi(x,y,z)-i\omega t}. \tag{2}$$

This example shows that the phase distortion is doubled through a conventional mirror and no phase-distortion correction is achieved. On the other hand, if a phase-conjugate mirror is used, the reflected and output waves are,

$$E''(x,y,z) = R_{pc} A_0(x,y,z)e^{-ikz-i\phi(x,y,z)-i\omega t}, \tag{3}$$

$$E'''(x,y,z) = R_{pc} A_0(x,y,z)e^{-ikz-i\phi(x,y,z)+i\phi(x,y,z)-i\omega t} = R_{pc} A_0(x,y,z)e^{-ikz-i\omega t}. \tag{4}$$

The output wave in this scenario cancels the distortions generated by the phase delay. Several different methods can be be used to generate a phase-conjugate mirror. Here, a degenerate four-wave mixing process was chosen due to its compatibility with both picosecond and nanosecond configurations.

B. Degenerate Four-wave Mixing

The degenerate four-wave mixing phase-conjugate signal [33, 34] is generated when a nonlinear medium is pumped by two planar counter-propagating beams and an imaging beam, as illustrated in Fig. 2. The three incident beams with frequency ω have electric fields of $E_1 = A_1(r)e^{ik_1\cdot r-i\omega t}$, $E_2 = A_2(r)e^{ik_2\cdot r-i\omega t}$, and $E_3 = A_3(x,y,z)e^{ik_3\cdot z-i\omega t}$. When these three beams interact in the medium, a fourth beam is generated. From phase matching, we have $k_1 + k_2 = k_3 + k_4$ which gives $k_3 = -k_4$ because the pump beams are counter-propagating ($k_1 = -k_2$). Phase matching dictates that the phase-conjugate beam is propagating in the opposite direction as the E_3 with a third-order nonlinear electric polarization of [33],

$$P_4^{(3)} = \epsilon_0 \chi_e^{(3)} A_1 A_2 A_3^* e^{ik_3\cdot z-i\omega t}, \tag{5}$$

where $\chi_e^{(3)} = \chi^{(3)}(\omega,\omega,-\omega)$ is the effective third-order nonlinear susceptibility. The equations describing the amplitude variation along the z-axis can be approximated as,

$$\frac{dA_3^*(z)}{dz} = i\gamma^* A_4(z), \qquad \frac{dA_4(z)}{dz} = i\gamma A_3^*(z), \qquad \text{and} \qquad \gamma = \frac{\omega}{2cn_0(\omega)}\chi_e^{(3)} A_1 A_2. \tag{6}$$

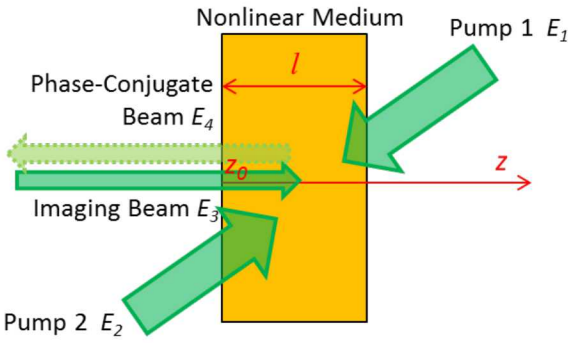

Fig. 2 A simple diagram of the degenerate four-wave-mixing process is shown.

Assuming that the pump beam amplitudes stay constant, the magnitude of the phase-conjugate signal evaluated at one end of the media is,

$$A_4(z_0) = -i\frac{\gamma}{|\gamma|}\tan(|\gamma|l)A_3^*(z_0). \tag{7}$$

Here, A_4 is proportional to A_3^*, which is the complex conjugate of the imaging beam A_3. Therefore, the electric field of the phase-conjugate wave assuming small signal gains is $E_4 = A_4(x, y, z)e^{-ik_3\cdot z - i\omega t}$. The resulting reflectivity of the phase-conjugate mirror is,

$$R_{pc} = |A_4(0)|^2/|A_3(0)|^2 = tan^2(|\gamma|l), \tag{8}$$

where l is the interaction length of the pump beams and imaging beam. From this equation, it is clear that the reflectivity of the phase-conjugate mirror depends heavily on the third-order nonlinear susceptibility value, the interaction length, and the amplitude of the two pump beams A_1 and A_2.

C. Digital In-line Holography

In digital in-line holography, holograms are created by the coherent interference of light scattered by objects $E_s(x, y)$ with the co-propagating un-scattered reference beam $E_r(x, y)$. The interference patterns are measured at the holography image plane and can be numerically refocused to the optical depth z using,

$$E_h(x, y, z) = \left[h(x, y)E_r^*(x, y)\right] \otimes g(x, y, z), \tag{9}$$

Where $E_h(x, y, z)$ is the reconstructed complex amplitude, $h(x, y) = |E_s + E_r|^2$ is the intensity of the recorded hologram at the holography image plane, E_r^* is the planar conjugate reference wave, $\otimes$ is the convolution operator, and g is the diffraction kernel. The refocused image at any depth z can be visualized using the amplitude $A_h = |E_h|$. Digital in-line holograms are collected out of focus, with the focal plane placed some distance from the object. In order to determine the z location of each object, the images are numerically refocused and a hybrid focus metric is applied (that maximizes the edge sharpness and minimizes the amplitude) [1, 2]. An example DIH measurement with a single horizontal wire is illustrated in Fig. 3. The raw DIH image at z = 97 mm (the hologram is collected out of focus) shows interference

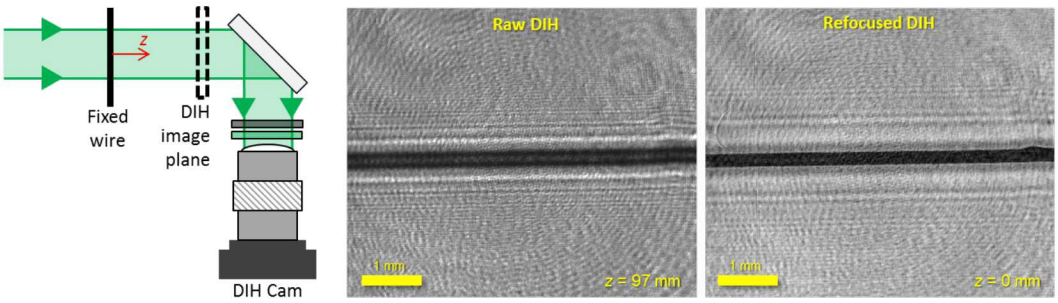

Fig. 3 Raw (at z = 97 mm) and numerically refocused (at z = 0 mm) DIH images of a fixed wire are shown.

patterns with no clear wire edges. When the same data is numerically refocused to $z = 0$ mm, the edges of the wire become sharper indicating the in-focus z-location.

III. Experimental Apparatus

Initial PCDIH and DIH measurements were conducted with a 20 Hz regeneratively-amplified picosecond laser (Ekspla PL2231C-20, 20 Hz, 60 ps, 532 nm, >15 mJ/pulse) as shown in Fig. 4. For later ultra-high-speed experiments, a custom modified Spectral Energies QuasiModo nanosecond pulse-burst laser is used to generate laser light with pulse durations of ≤7 ns at 532 nm and burst durations of 1.5 ms or lower (to maximize flashlamp voltage and energy per pulse). The laser provides one burst every 12 seconds. Custom software upgrades were also implemented to operate the laser at higher repetition rates. This laser contains a pulsed seed source with a 2 GHz bandwidth, two double-pass diode-pumped amplification stages, two double-pass 9 mm diameter flashlamp-pumped amplification stages, and two single-pass 12 mm diameter flashlamp-pumped amplification stages. The 1064 nm light is then passed through a telescope and doubled to 532 nm through a 30 mm long LBO crystal.

The 532 nm light exiting the lasers is passed through a two-stage attenuator (to control laser intensity) consisting of half-wave plates and thin film polarizers. Then, the light enters a 15 mm diameter Electro-Optics Technology isolator and a vertical periscope (not illustrated). The laser light is subsequently split into a imaging beam and two pump beams. The imaging beam passes through a delay stage, a vacuum pinhole spatial filter (300 mm FL lenses, 100 μm pinhole), and a 3× beam expander. The light then passes through the PCDIH camera pick-off mirror (5% reflectivity), the object area, and a second DIH pick-off mirror (5% reflectivity). The remaining light is then focused through a heavy fluorocarbon 3M FC-72 fluid cell (AR coated, 1 mm thick windows, 10 mm thick cell). The FC-72 liquid is used due to its low toxicity and high phase-conjugate mirror reflectivity [35].

The two counter-propagating pump beams are also delayed and passed through the cell so that all three beams intersect just before the focal point of the imaging beam. This configuration prevents breakdown inside the cell and damage to the cell windows. The pump beams pass through telescopes in order to decrease beam-size, control divergence, and increase energy density. The angle between the pump beams and the imaging beam is 23°. Inside the cell, the phase-conjugate signal is generated and is illustrated as dotted green lines. The polarizations of pump 1, pump 2, imaging beam, and phase-conjugate beam are p-, s-, p-, and s-polarized, respectively. Overlap of the two counter-propagating pump beams is critical to producing overlap of the imaging beam and phase-conjugate signal. The phase-conjugate signal then back propagates along the imaging path before it is directed into the PCDIH camera. Additional neutral density filters and laserline filters are added to control signal intensity and block unwanted emissions from plasmas and explosives.

Due to the longer pulse durations of nanosecond lasers, a more efficient configuration similar to [25, 36] can also be

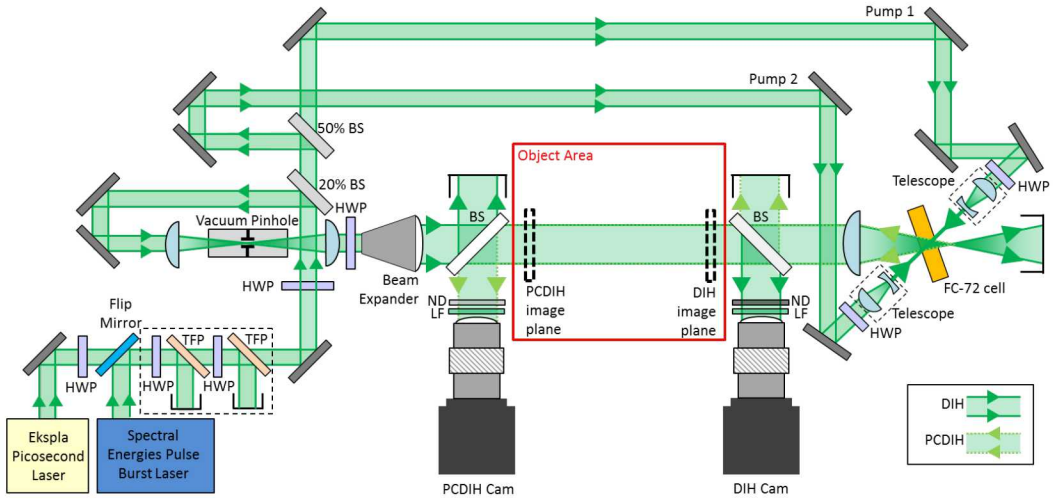

Fig. 4 Simplified setup for PCDIH using a picosecond laser or a nanosecond pulse-burst laser. For holography, the image planes are placed out of focus. (HWP–half wave plate, TFP–thin-film polarizer, BS–beam splitter, ND–neutral density filter, LF–laserline filter 0.2 nm FWHM bandwidth)

used. In this design, the laser light is split into a single pump beam and a single imaging beam. The single pump 1 beam passes through the cell and then into a quarter wave plate and 90° mirror, which rotates the polarization to create the pump 2 beam that passes back through the cell. The same beam is reused for both pumps in order to direct more energy into the pump beams.

For 20 Hz imaging, LaVision sCMOS (2560 × 2160 pixels, 6.5 μm pixel pitch, 16-bit depth) cameras are used to acquire data through Infinity K2 DistaMax long distance microscopes. For ultra-high-speed applications, Shimadzu HPV-X2 cameras were utilized. These cameras are 400 × 250 pixels with a 32 μm pixel pitch. They are capable of recording up to 128 frames in full-frame mode with a 10-bit depth at up to 5 MHz. Since supersonic, hypersonic, and explosive events are fast, this number of frames was sufficient for capturing the event. In addition, since these events are short, laser pulse synchronization with the camera was not required.

IV. Single-shot 20 Hz Measurements with a Picosecond Laser

A. Stationary Supersonic Shock-waves

To better understand the interaction of phase-distortions with and without the phase-conjugate mirror, data was first collected via normal imaging, as illustrated in the experimental setup shown in Fig. 5. Since this first experiment explores imaging results rather than holography, the imaging planes of the PC camera and normal camera are placed at the center of a stationary shock-wave generated by a supersonic air jet (over-expanded jet, design Mach number of 3.7, 6.35 mm nozzle outlet, stagnation pressure 4.8 MPa, atmospheric pressure 84 kPa).

Results from left to right show the view from the normal camera, the view from the phase-conjugate camera, and the view when the phase-conjugate mirror and lens are replaced with an ordinary mirror. The in-focus images from the normal camera show sharp and clear shock-waves due to light refraction off the shock-wave edges. Some turbulent disturbances are also clearly visible. The phase-conjugate image not only shows the edges of the shock-waves and turbulent disturbances but also shows dark shadows at these edges, making them more clearly visible. This is likely due to two different effects. First, because the phase-conjugate mirror design double passes light through a disturbance, absorption is higher for the phase-conjugate image. Second, the phase-conjugate mirror design can be configured to reject light that is slightly refracted by the curvature of a shock-wave or turbulent disturbance.

These two images can then be compared to the final image taken with the phase-conjugate camera with the lens and cell replaced with an ordinary mirror. Since an ordinary mirror does not correct for phase delays or interference patterns generated during the first pass, the image is much more distorted with stronger interference patterns. Additionally, the angle of incidence and angle of reflection for a phase-conjugate mirror is the same, while the two angles are different for an ordinary mirror. Thus, the image taken with the ordinary mirror is a combination of the strong out-of-focus interference patterns with low spatial frequency (due to the light refracted during the first pass through the shock-wave) and the sharp in-focus shock-wave edges (due to the light refracted during the second pass through the shock-wave). This example highlights the differences between a phase-conjugate mirror and an ordinary mirror.

To investigate effects from in-line holography, the focal planes of the two cameras are moved back as illustrated in Fig. 6 to a distance of ~97 mm from the wire such that the magnification of the two systems match. The top row of

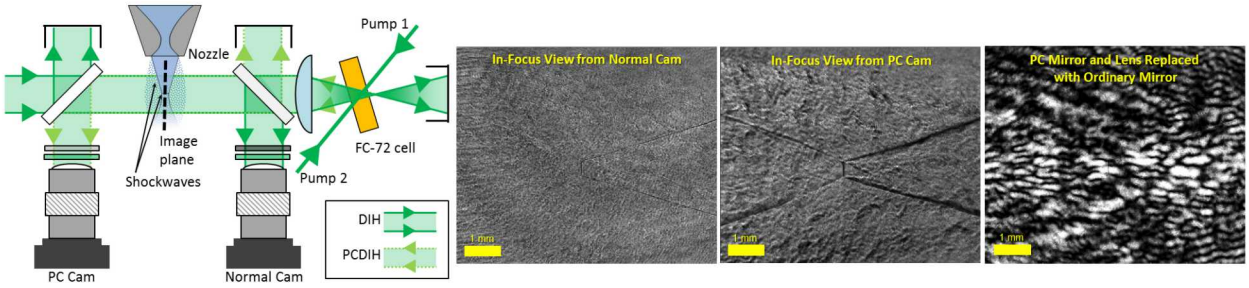

Fig. 5 A comparison of phase-conjugate and normal in-focus imaging through a supersonic jet is shown. Results from left to right show single-shot views from the in-focus normal camera, the phase-conjugate camera, and the phase-conjugate camera when the phase-conjugate mirror and lens are replaced with a 90° ordinary mirror.

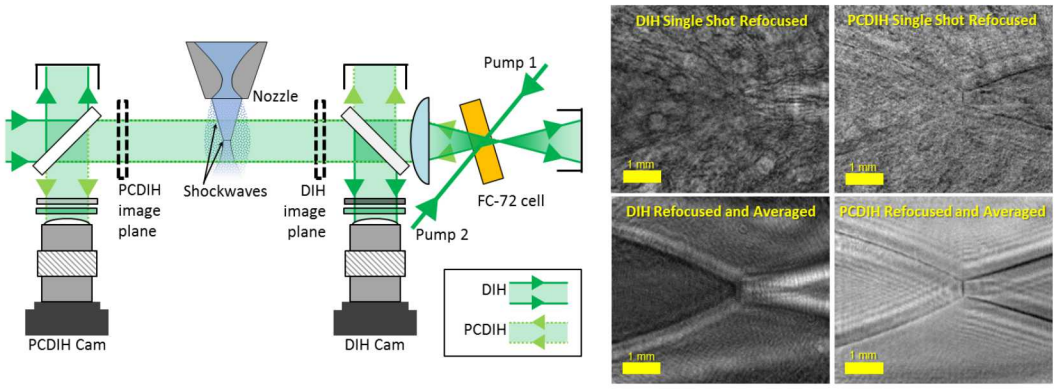

Fig. 6 A PCDIH and DIH imaging setup is illustrated to obtain holograms of shock-waves in a supersonic jet. This experiment is identical to Fig. 5 except for the location of the image planes. The top row shows single-shot refocused holograms illustrating shock-wave and local turbulence distortions. The bottom row shows averaged (500 images) refocused holograms where turbulent distortions are removed and only shock-wave edges are visible.

images shows single-shot holograms that are numerically refocused to the centerline of the shock-wave. The PCDIH image shows clearly-visible shock-wave edges while the DIH images are unable to be refocused. When Fig. 5 and 6 are compared, it is clear that the quality degrades when comparing imaging techniques to holographic techniques that require numerical refocusing. Some of this image degradation is due to the presence of the virtual image inherent in DIH techniques and some of the degradation is due to the refocusing of turbulent structures.

The effect of random turbulent structures can be removed by averaging multiple shots through the stationary shock-waves. The bottom row of images in Fig. 6 are averaged from 500 different shots. Even without the turbulence effects, it is clear that the averaged PCDIH refocused image shows all the shock-wave edges clearly and the averaged traditional DIH refocused image does not show clear shock-wave edges. This experiment illustrates the effect of phase delays on DIH images. The inability to refocus DIH images is due to the dominance of the phase-delay distortions (from jet density gradients) over the interference patterns generated by refraction at the shock-wave edges. In PCDIH, only the refraction effects are present and the phase-delay distortions are canceled, allowing shock-wave edges to be refocused.

B. Laser-spark Plasma-generated Shock-waves

The picosecond PCDIH setup is next tested in a laser-spark plasma-generated shock-wave environment. In this experiment, the effect of distortions on absorptive objects (in this case a 200 μm diameter fixed wire) is tested, as illustrated in Fig. 7. For this experiment, the focal planes for the DIH and PCDIH systems were placed ~61 mm from the wire. A focused nanosecond laser (Continuum Surelite III, 10 Hz, 1064 nm, 5 ns pulse duration, 400 mJ per pulse) was used to generate a spark via laser-induced breakdown of air at a distance of ~15 mm from the wire to produce plasma-generated shock-waves that distort the appearance of the wire. The holograms are then captured ~400 ns after the generation of the laser spark.

In the series of results in Fig. 7, the top row of images show the raw DIH measurement of the wire, the raw PCDIH image of the wire, the wire and shock-wave imaged by DIH, and wire and shock-wave imaged by PCDIH. The row directly below shows images numerically refocused to the z-plane of the wire. The traditional DIH images show wire edges that are completely distorted by phase-delays while the PCDIH images show significantly less distortions. The effect of phase-delay distortions on DIH and PCDIH images over 500 different laser-spark shots can be quantitatively compared. When using a metric comparing the standard deviation of the tracked wire edges, results indicate that DIH images show ~8× more distortion than the PCDIH [24]. When the laser spark is moved to the opposite side of the wire, results show that DIH is still significantly more distorted than the PCDIH image by ~11.7× [24].

When comparing the spatial resolution of DIH with PCDIH, results show that the standard deviation of the wire edge with no spark is 0.6 μm for DIH and 1.9 μm for PCDIH [24]. This indicates that the DIH image edges have higher spatial resolution. This effect is most likely due to the shadow generated by the laser beam absorption during the first pass over the wire. This shadow overlaps with the object during the second pass but can be slightly larger than the object due to diffraction pattern propagation, non-overlapped imaging and phase-conjugate beams, and beam divergence.

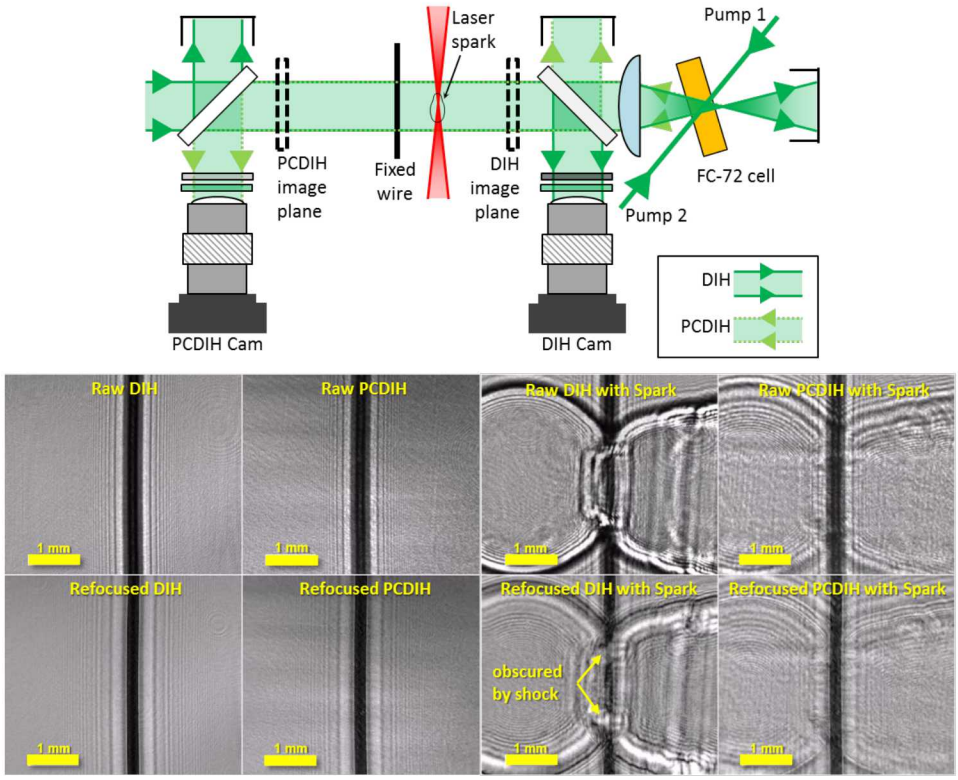

Fig. 7 Single-shot holograms of a fixed wire and laser-spark plasma-generated shock-wave are illustrated. The top row of images shows the raw DIH image of the wire, raw PCDIH image of the wire, wire with a spark imaged with traditional DIH, and wire with a spark imaged with PCDIH. The bottom row shows the same holograms refocused to the plane of the wire.

Finally, when comparing the dynamic range of shock-waves in the two images, the interference patterns generated by the shock-waves appear brighter in DIH than PCDIH. This effect is due to phase delays caused by the density gradients and shape of the shock-wave. These phase effects that cause bright interference patterns are reduced or minimized by the phase-conjugate mirror for PCDIH images, leading to weaker interference patterns.

C. Explosively-generated Hypersonic Fragments

Single-shot images of a fragmenting explosive detonator are also obtained using the picosecond laser PCDIH setup, as shown in Fig. 8. In these experiments, a polycarbonate boombox is used to protect the optics inside the object area and to contain the fragments [24]. The top of the detonator is covered by an aluminum foil and when the explosive ignites, fragments of aluminum are launched at approximately 2.5 km/s or Mach 7.2 [37]. These hypersonic fragments generate strong shock-waves as they travel, which obscure other fragments that are traveling slightly behind the leading fragments [37]. In order to better understand the dynamics of the system, it is important to image and track the leading fragments, the lagging fragments, and the interaction of the shock-waves.

Results in Fig. 8 shows a traditional DIH image distorted by shock-wave phase-delay distortions, the PCDIH image with phase-delay distortions minimized, and the tracked PCDIH image with each fragment refocused to its respective focal plane. One particularly interesting comparison can be made between the DIH and PCDIH images for a long and tall fragment near the center of the images. This fragment is completely obscured in the DIH image by shock-wave distortions but is easily visible and refocusable in the PCDIH image. This example illustrates that the technique can be utilized for 3D object tracking in explosive environments.

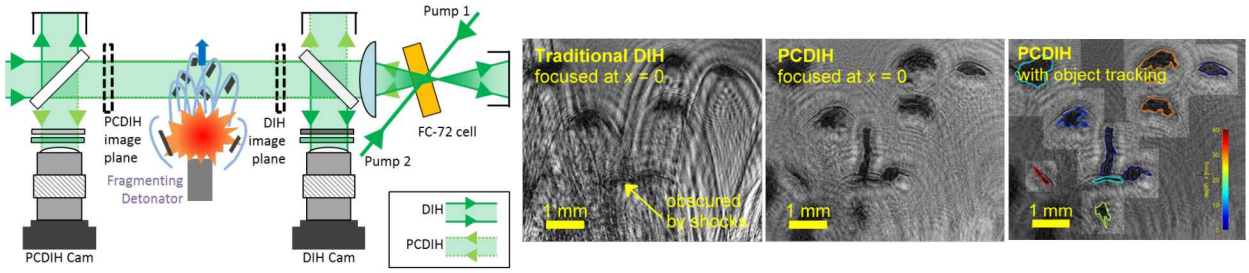

Fig. 8 Holograms of a fragmenting detonator (pointing upward) are illustrated. Results from left to right show the refocused traditional DIH image of objects obscured by shock-wave distortions, a simultaneously-obtained PCDIH image with shock-wave distortions minimized, and tracked PCDIH images showing each fragment in its respective focal plane. Images provided courtesy of [24].

V. Time-resolved Ultra-high-speed Measurements with a Pulse-burst Laser

The low repetition-rate results from the high-beam-quality picosecond laser show many of the main benefits of the PCDIH technique. However, a pulse-burst laser is required to obtain images at ultra-high-speeds. For a 20 Hz PCDIH system, only a single frame can be obtained per experiment. In many extreme environments, there can be significant variation from test to test. Therefore, time-resolved measurements are essential for gathering data via 3D object or shock-wave tracking.

For pulse-burst lasers, the energy per pulse drops significantly as ultra-high speeds. This is due, in part, to the increase in the repetition rate. Since the maximum energy per burst in the amplification stages is fixed, having more pulses decreases the energy per pulse at 1064 nm. The lower pulse energy at 1064 nm then decreases the nonlinear second harmonic conversion efficiency, which further decreases the 532 nm pulse energy. In addition, the phase-conjugate mirror relies on a nonlinear four-wave mixing process. Therefore, the phase-conjugate mirror reflectivity also decreases as the pulse energies decrease. Finally, the conversion efficiency of nanosecond lasers is lower than picosecond lasers with comparable pulse energies due to differences in their relative peak intensities. These factors contribute to some of the challenges associated with implementing PCDIH at ultra-high speeds.

A. Laser-spark Plasma-generated Shock-waves

The nanosecond pulse-burst laser was utilized in the laser-spark plasma-generated shock-wave experiment. A horizontal wire and a vertical wire were placed on either side of the shock-wave at distances of ~12 mm from the laser spark. The image planes of the cameras are placed ~30 mm from the laser spark. Figure 9 illustrates the experiment conducted at 500 kHz with results refocused to the vertical wire plane and refocused to the horizontal wire plane. The

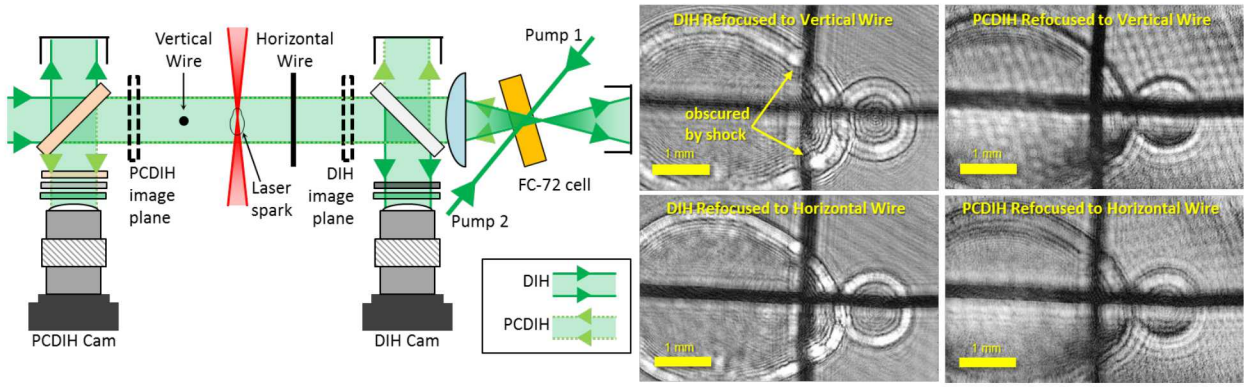

Fig. 9 Holograms from the pulse-burst nanosecond laser operating at 500 kHz are illustrated for a laser-spark plasma-generated shock-wave. The laser spark is place between a vertical and horizontal wire. The tradition DIH images show the vertical wire distorted by the shock-wave. The PCDIH images shows no distortion of the refocused wires.

DIH images show the vertical wire distorted by the shock-wave. The corresponding PCDIH images, on the other hand, show significantly reduced distortions.

This dataset also illustrates some differences between the picosecond laser implementation and the nanosecond pulse-burst implementation. The overall spatial resolution of the nanosecond pulse-burst results is lower than the picosecond laser data because the ultra-high-speed camera has fewer pixels. The beam quality of the nanosecond pulse-burst is also poorer than the regeneratively amplified picosecond laser. Despite these drawbacks, the nanosecond pulse-burst implementation still clearly demonstrates successful numerical refocusing of the hologram and phase-distortion cancellation.

B. Shock-wave Edge Enhancement

The four-wave-mixing phase-conjugate configuration can be used to remove phase distortions, but can also be altered to preferentially enhance shock-wave edges. Figure 10 illustrates an example of conventional DIH compared with PCDIH with a longer focal length lens (300 mm FL) and PCDIH with a shorter focal length lens (125 mm FL). With the longer focal length lens, a strong shadow is noted near the shock-wave edges. For the shorter focal length lens, the shadow intensity is significantly reduced.

A possible mechanism for this edge enhancement effect is schematically illustrated in in Fig. 11. When light passes through a density gradient with some curvature, the light is refracted slightly before exiting the density gradient. When the light is focused through the lens, the refracted light is focused at a slightly different position than the un-refracted light. Depending on the position of the phase-conjugate mirror cell and size of the pump beams, the refracted light and un-refracted light are preferentially amplified and reflected to different degrees depending on differences in their interaction lengths l (see Eq.(8)). By varying the focal length of the lens, the focal point of the refracted light can fall far outside the phase-conjugate cell, thereby altering the interaction length and creating a darker phase-conjugate mirror signal in areas of the density gradient that refract light the most. This effect is controlled by the size of the pump beams, focal length of the lens, the density difference between the gases inside and outside the shock-wave, the size and curvature of the shock-wave, and the distances between the density gradient, lens, and cell. This effect has some similarity with schlieren and shadowgraphy techniques except that it utilizes a non-linear effect and is conducted with coherent light. In addition, it is able to numerically refocus to a shock-wave edge and can be used to determine the z-location of the shock-wave. Future work modeling this effect can help determine the sensitivity of the technique and if three-dimensional shock-wave shape can be extracted from gradients in the shadow intensity.

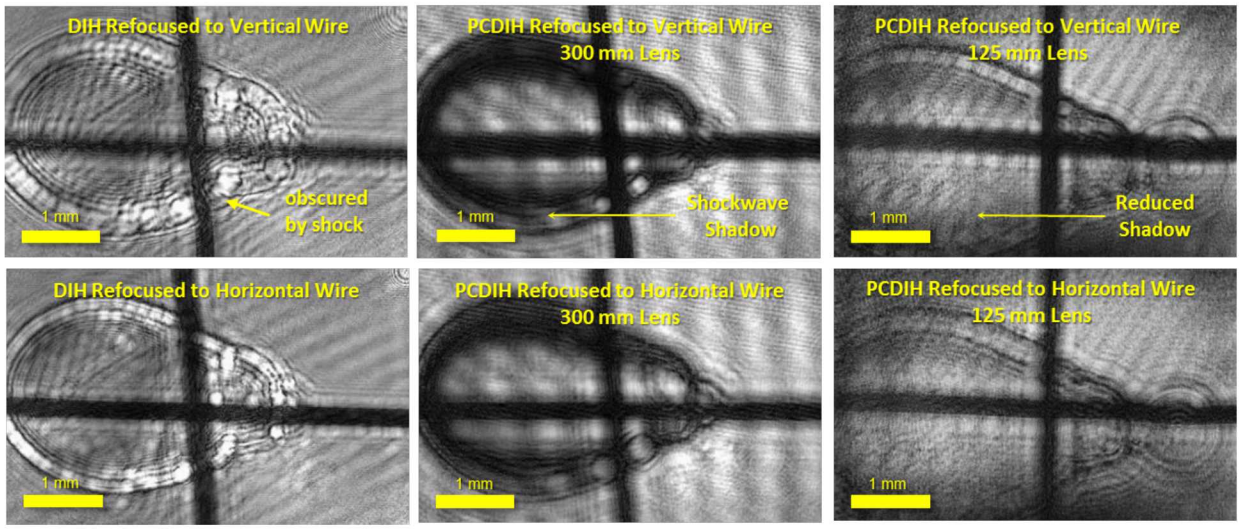

Fig. 10 Density gradient edges are enhanced using degenerate four-wave-mixing PCDIH collected at 500 kHz. From left to right, images are shown of traditional DIH, PCDIH using a long focal-length lens (300 mm FL), and PCDIH using a shorter focal-length lens (125 mm FL).

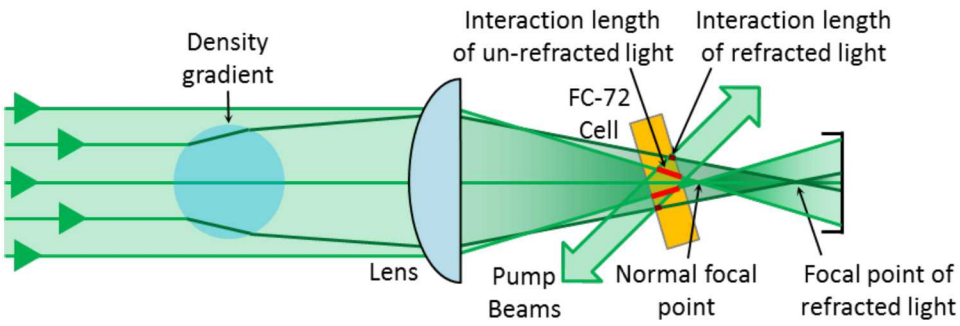

Fig. 11 A schematic of the edge enhancement mechanism is illustrated. The light refracted by the density gradient and the un-refracted light focus to different positions. This determines the interaction lengths (red lines for un-refracted light, dark red lines for refracted light) between the imaging beam and the pump beams, which determines the amount of phase-conjugate signal generated. The relative location of the focal-points and the phase-conjugate cell determines the degree of edge enhancement.

VI. Conclusion

Ultra-high-speed PCDIH is essential for making time-resolved measurements of objects distorted by shock-waves or other types of density gradients. This paper demonstrates the implementation of this technique at up to 500 kHz with a pulse burst laser and ultra-high-speed cameras. Implementations of PCDIH in this paper demonstrate how the technique successfully removes interference patterns generated by phase-distortions. However, PCDIH does have a few drawbacks. Compared to DIH, the PCDIH technique has higher setup complexity. When repetition rates increase, the signal-to-noise levels drop and the image quality degrades. Due to the back-reflecting configuration, PCDIH is also more susceptible to specular reflections from objects. Nevertheless, this work demonstrates several applications of the technique in challenging environments from imaging shock-waves in supersonic jets, correcting phase distortions in laser-spark plasma-generated shock-waves, and tracking explosively-generated hypersonic fragments.

Acknowledgments

We would like to thank Dr. Phillip L. Reu, Dr. Steven Beresh, Seth Spitzer, Russell Spillers, Marley Kunzler, Andres N. Baca and the Explosives Technologies Group for their assistance with experimental equipment. This work was supported by the Exploratory Express Laboratory Directed Research and Development program at Sandia National Laboratories, which is a multimission laboratory managed and operated by National Technology and Engineering Solutions of Sandia, LLC., a wholly owned subsidiary of Honeywell International, Inc., for the U.S. Department of Energy's National Nuclear Security Administration under contract DE-NA0003525.

References

[1] Guildenbecher, D. R., Gao, J., Reu, P. L., and Chen, J., "Digital Holography Simulations and Experiments to Quantify the Accuracy of 3D Particle Location and 2D Sizing Using a Proposed Hybrid Method," *Appl. Opt.*, Vol. 52, No. 16, 2013, pp. 3790–3801.

[2] Guildenbecher, D. R., Reu, P. L., Stauffacher, H. L., and Grasser, T. W., "Accurate Measurement of Out-of-plane Particle Displacement from the Cross Correlation of Sequential Digital In-line Holograms," *Opt. Lett.*, Vol. 38, No. 20, 2013, pp. 4015–4018.

[3] Buchmann, N. A., Atkinson, C., and Soria, J., "Ultra-high-speed Tomographic Digital Holographic Velocimetry in Supersonic Particle-laden Jet Flows," *Meas. Sci. Technol.*, Vol. 24, 2013, p. 024005.

[4] Chen, Y., Wagner, J. L., Farias, P. A., DeMauro, E. P., and Guildenbecher, D. R., "Galinstan Liquid Metal Breakup and Droplet Formation in a Shock-induced Cross-flow," *Int. J. Multiphase Flow*, Vol. 106, 2018, pp. 147–163.

[5] Chen, Y., DeMauro, E. P., Wagner, J. L., Arienti, M., Guildenbecher, D. R., Farias, P. A., Grasser, T. W., Sanderson, P. D., Albert, S. W., Turpin, A. M., Sealy, W., and Ketchum, R. S., "Aerodynamic Breakup and Secondary Drop Formation for a Liquid Metal Column in a Shock-Induced Cross-Flow," *55th AIAA Aerospace Sciences Meeting, AIAA SciTech*, 2017. AIAA-2017-1892.

[6] Guildenbecher, D. R., Wagner, J. L., Olles, J. D., Chen, Y., DeMauro, E. P., Farias, P. A., Grasser, T. W., and Sojka, P. E., "kHz Rate Digital In-Line Holography Applied to Quantify Secondary Droplets from the Aerodynamic Breakup of a Liquid Column in a Shock-Tube," *54th AIAA Aerospace Sciences Meeting, AIAA SciTech*, 2016. AIAA-2016-1044.

[7] Guildenbecher, D. R., Cooper, M. A., and Sojka, P. E., "High-speed (20 kHz) Digital In-line Holography for Transient Particle Tracking and Sizing in Multiphase Flows," *Appl. Opt.*, Vol. 55, No. 11, 2016, pp. 2892–2903.

[8] Chen, Y., Wagner, J. L., Farias, P. A., and Guildenbecher, D. R., "Study of Galinstan Liquid Metal Breakup Using Backlit Imaging and Digital In-line Holography," *14th International Conference on Liquid Atomization and Spray Systems (ICLASS)*, 2018.

[9] Chen, Y., Guildenbecher, D. R., Hoffmeister, K. N. G., Cooper, M. A., Stauffacher, H. L., Oliver, M. S., and Washburn, E. B., "Study of Aluminum Particle Combustion in Solid Propellant Plumes using Digital In-line Holography and Imaging Pyrometry," *Combust. Flame*, Vol. 182C, 2017, pp. 225–237.

[10] Chen, Y., Guildenbecher, D. R., Hoffmeister, K. N. G., and Sojka, P. E., "Digital Imaging Holography and Pyrometry of Aluminum Drop Combustion in Solid Propellant Plumes," *Proceedings of the Imaging and Applied Optics Conference: Laser Applications to Chemical, Security and Environmental Analysis*, 2016. LT4F.2.

[11] Chen, Y., Heyborne, J. D., and Guildenbecher, D. R., "Time-resolved Digital In-line Holography and Pyrometry for Aluminized Solid Rocket Propellants," *Proceedings of the Imaging and Applied Optics Conference: Laser Applications to Chemical, Security and Environmental Analysis*, 2018. LTu3C.5.

[12] Guildenbecher, D. R., Cooper, M. A., Gill, W., Stauffacher, H. L., Oliver, M. S., and Grasser, T. W., "Quantitative, Three-Dimensional Imaging of Aluminum Drop Combustion in Solid Propellant Plumes via Digital In-Line Holography," *Opt. Lett.*, Vol. 39, No. 17, 2014, pp. 5126–5129.

[13] Powell, M. S., Gunduz, I. W., Shang, W., Chen, J., Son, S. F., Chen, Y., and Guildenbecher, D. R., "Agglomerate Sizing in Aluminized Propellants Using Digital Inline Holography and Traditional Diagnostics," *J. Propul. Power*, Vol. 34, No. 4, 2018, pp. 1002–1014.

[14] Marrinan, D. P., Fuest, F., and Sutton, J. A., "Spatial Resolution-preserving Retroreflection for Gas-phase Laser Scattering Measurements in Turbulent Flames using a Phase-conjugate Mirror," *Opt. Lett.*, Vol. 41, No. 3, 2016, pp. 468–471.

[15] Bloom, D. M., and Bjorklund, G. C., "Conjugate Wave-front Generation and Image Reconstruction by Four-wave Mixing," *Appl. Phys. Lett.*, Vol. 31, No. 9, 1977, pp. 592–594.

[16] Yarrison-Rice, J. M., Sharp, E. J., Wood, G. L., Salamo, G. J., Klank, R., and Neurgaonkar, R. R., "High-resolution Phase-conjugate Imaging in Double-pumped Phase Conjugators," *Appl. Opt.*, Vol. 34, No. 32, 1995, pp. 7597–7603.

[17] Devaux, F., le Tolguenec, G., and Lantz, E., "Phase Conjugate Imaging by Type II Parametric Amplification," *Opt. Commun.*, Vol. 147, 1998, pp. 309–312.

[18] Thurow, B., Jiang, N., Samimy, M., and Lempert, W., "Narrow-linewidth Megahertz-rate Pulse-burst Laser for High-speed Flow Diagnostics," *Appl. Opt.*, Vol. 43, No. 26, 2004, pp. 5064–5073.

[19] Fischer, B., and Sternklar, S., "Image Transmission and Interferometry with Multimode Fibers using Self-pumped Phase Conjugation," *Appl. Phys. Lett.*, Vol. 46, No. 2, 1985, pp. 113–114.

[20] Kogelnik, H., "Imaging of Optical Modes–Resonators with Internal Lenses," *Bell Syst. Tech. J.*, Vol. 44, No. 3, 1965, pp. 455–494.

[21] Shibukawa, A., Okamoto, A., Goto, Y., Honma, S., and Tomita, A., "Digital Phase Conjugate Mirror by Parallel Arrangement of Two Phase-only Spatial Light Modulators," *Opt. Express*, Vol. 22, No. 10, 2014, pp. 11918–11929.

[22] Hillman, T. R., Yamauchi, T., Choi, W., Dasari, R. R., Feld, M. S., Park, Y., and Yaqoob, Z., "Digital Optical Phase Conjugation for Delivering Two-dimensional Images through Turbid Media," *Sci. Rep.*, Vol. 3, 2013.

[23] Toda, S., Kato, Y., Kudo, N., and Shimizu, K., "Effects of Digital Phase-conjugate Light Intensity on Time-reversal Imaging through Animal Tissue," *Biomed. Opt. Express*, Vol. 9, No. 4, 2018.

[24] Guildenbecher, D. R., Hoffmeister, K. N. G., Kunzler, W. M., Richardson, D. R., and Kearney, S. P., "Phase Conjugate Digital Inline Holography (PCDIH)," *Opt. Lett.*, Vol. 43, No. 4, 2018, pp. 803–806.

[25] Hoffmeister, K. N. G., Kearney, S. P., and Guildenbecher, D. R., "Optical Phase Conjugate Digital Inline Holography for Correcting Aberations in Particle-laden Flames," *54th AIAA Aerospace Sciences Meeting, AIAA SciTech*, 2016. AIAA-2016-1046.

[26] Beresh, S., Kearney, S., Wagner, J., Guildenbecher, D., Henfling, J., Spillers, R., Pruett, B., Jiang, N., Slipchenko, M., Mance, J., and Roy, S., "Pulse-burst PIV in a High-speed Wind Tunnel," *Meas. Sci. Technol.*, Vol. 26, No. 9, 2015, pp. 095305–1 – 095305–13.

[27] Michael, J. B., Venkateswaran, P., Shaddix, C. R., and Meyer, T. R., "Effects of Repetitive Pulsing on Multi-kHz Planar Laser-induced Incandescence Imaging in Laminar and Turbulent Flames," *Appl. Opt.*, Vol. 54, No. 11, 2015, pp. 3331–3344.

[28] Meyer, T. R., Halls, B. R., Jiang, N., Slipchenko, M. N., Roy, S., and Gord, J. R., "High-speed, Three-dimensional Tomographic Laser-induced Incandescence Imaging of Soot Volume Fraction in Turbulent Flames," *Opt. Express*, Vol. 24, No. 26, 2016, pp. 29547–29555.

[29] Roy, S., Hsu, P. S., Jiang, N., Slipchenko, M. N., and Gord, J. R., "100-kHz-rate Gas-phase Thermometry using 100-ps Pulses from a Burst-mode Laser," *Opt. Lett.*, Vol. 40, No. 21, 2015, pp. 5125–5128.

[30] Fuest, F., Papageorge, M. J., Lempert, W. R., and Sutton, J. A., "Ultrahigh Laser Pulse Energy and Power Generation at 10kHz," *Opt. Lett.*, Vol. 37, No. 15, 2012, pp. 3231–3233.

[31] Smyser, M. E., Rahman, K. A., Slipchenko, M. N., Roy, S., and Meyer, T. R., "Compact Burst-mode Nd:YAG Laser for kHz-MHz Bandwidth Velocity and Species Measurements," *Opt. Lett.*, Vol. 43, No. 4, 2018, pp. 735–738.

[32] Sugawa, S., Kuroda, R., Takeda, T., Shao, F., Miyauchi, K., and Tochigi, Y., "A 20Mfps Global Shutter CMOS Image Sensor with Improved Sensitivity and Power Consumption," *International Image Sensor Workshop*, 2015, pp. 166–169.

[33] He, G. S., "Optical Phase Conjugation: Principles, Techniques and Applications," *Prog. Quant. Electron.*, Vol. 26, 2002, pp. 131–191.

[34] Hellwarth, R. W., "Generation of Time-reversed Wave Fronts by Nonlinear Refraction," *J. Opt. Soc. Am.*, Vol. A67, No. 1, 1977, pp. 1–3.

[35] Yoshida, H., Kmetik, V., Fujita, H., Nakatsuka, M., Yamanaka, T., and Yoshida, K., "Heavy Fluorocarbon Liquids for a Phase-conjugated Stimulated Brillouin Scattering Mirror," *Appl. Opt.*, Vol. 36, No. 16, 1997, pp. 3739–3744.

[36] Van Wonterghem, B., Dutton, T. E., Saltiel, S. M., and Rentzepis, P. M., "Optical Phase Conjugation Reflectivity and Fidelity in CS2 by Picosecond Pulse Four Wave Mixing," *J. Appl. Phys.*, Vol. 64, 1988, pp. 4329–4333.

[37] Yeager, J. D., Bowden, P. R., Guildenbecher, D. R., and Olles, J. D., "Characterization of Hypervelocity Metal Fragments for Explosive Initiation," *J. Appl. Phys.*, Vol. 122, No. 3, 2017, p. 035901.